Slow-slip evolves into megathrust earthquakes in 2D numerical simulations

Paul Segall[1] and Andrew M. Bradley[1]

Received 21 June 2012; revised 10 August 2012; accepted 14 August 2012; published 28 September 2012.

[1] Slow slip events (SSE) in many subduction zones incrementally stress the adjacent locked megathrust, suggesting that they could potentially either trigger or evolve into damaging earthquakes. We explore this with 2D quasi-dynamic simulations with rate-state friction, dilatancy, and coupled 1D pore-fluid and heat transport. Steady-state weakening friction allows transient slip to nucleate, but is inhibited by dilatant strengthening and destabilized by thermal pressurization. SSE spontaneously nucleate in Low Effective-Stress Velocity-Weakening (LESVW) regions. If the dimension of the LESVW is relatively small the SSE are trapped at its updip end, imparting a strong stress concentration in the locked zone. After several centuries SSE penetrate into the region of higher effective stress, where thermal pressurization eventually leads to dynamic rupture. For larger LESVW regions SSE tend to increase in length with time; ultimately higher slip speeds enhance thermal weakening, leading to dynamic instability within the SSE zone. In both cases the onset of the ultimate SSE is essentially indistinguishable from preceding events. **Citation:** Segall, P., and A. M. Bradley (2012), Slow-slip evolves into megathrust earthquakes in 2D numerical simulations, *Geophys. Res. Lett.*, *39*, L18308, doi:10.1029/2012GL052811.

1. Introduction

[2] In Cascadia SSE are accompanied by tectonic tremor and are referred to as Episodic Tremor and Slip (ETS). Because ETS there, and in other subduction zones, occur down-dip of the locked megathrust, each event incrementally stresses the zone where damaging quakes nucleate. This suggests that the occurrence of ETS may be useful in anticipating damaging earthquakes [*Mazzotti and Adams*, 2004].

[3] Given that SSE in Cascadia have repeat times of 10–19 months [*Brudzinski and Allen*, 2007], and last a few weeks, one could argue that the probability of a damaging event increases by a factor of ~30 during ETS (14 months/2 weeks). Indeed, warnings have been issued in Canada during ETS events (http://www.ctv.ca/CTVNews/TopStories/20070202/bc_quake_070202). With the inter-event time for megathrust quakes of ~500 years [*Goldfinger et al.*, 2011] there would likely be hundreds of SSE before a large plate-boundary earthquake occurs.

[4] Earthquake nucleation is, however, time-dependent, which can cause the probability distribution of triggering times to be spread out relative to the inter-ETS period. In the theory of *Dieterich* [1994], the time for seismicity to decay to background levels following a step change in stress is denoted t_a. If t_a is relatively long compared to the duration of ETS events, the seismicity rate is not predicted to peak significantly during the transient. *Beeler* [2012] argues that this is likely to be the case (citing t_a of years to decades), such that earthquake probability is not significantly enhanced by periodic slow slip events.

[5] Nevertheless, triggered seismicity has been associated with SSE in some localities, including the Boso Peninsula of Japan, where slip events every ~6 years have been accompanied by earthquakes as large as M 5.3 [*Ozawa et al.*, 2007]. SSE beneath Kilauea volcano are accompanied by swarms of small earthquakes [*Segall et al.*, 2006]. The timing of the GPS displacements relative to the swarm onset, as well as their spatial relationship, suggest that the earthquakes were triggered by static stress changes; the swarm events were thus referred to as "co-shocks" of the SSE [*Segall et al.*, 2006]. The temporal evolution of the swarms is consistent with the SSE induced stress changes and t_a on the order of 10 days (based on nearby aftershocks).

[6] Our simulations show that SSE can evolve directly into dynamic events, rather than trigger a remote nucleation site, a possibility that appears not to have received much attention, although see *Dragert et al.* [2004].

2. Method

[7] We present models of dipping faults in an elastic half-space with depth variable friction and effective stress to represent SSE in subduction zones (Figure 1 in Text S1 in the auxiliary material).[1] Deformation is plane-strain, with slip in the x-direction, and the fault centered on $y = 0$; z measures depth from the free surface. Fault slip δ is the integral of inelastic shear strain across the fault zone $-h/2 \le y \le h/2$. Inelastic deformation within the fault zone is approximated by a friction law, with shear resistance the product of friction coefficient f and effective normal stress $\sigma - p(y = 0)$. We employ the radiation damping approximation of elastodynamics [*Rice*, 1993] such that the momentum balance on the fault is

$$\tau_0 + G_{\tau\delta}\delta - f(v,\theta)[\sigma + G_{\sigma\delta}\delta - p(y=0)] = \frac{\mu}{2v_s}v. \qquad (1)$$

Elastic Green's functions $G_{\tau\delta}$ and $G_{\sigma\delta}$ give the changes in shear and normal stress, respectively, due to slip (slip-to-normal stress coupling arises due to the free surface). τ_0, μ,

[1]Department of Geophysics, Stanford University, Stanford, California, USA.

Corresponding author: P. Segall, Department of Geophysics, Stanford University, Stanford, CA 94305, USA. (segall@stanford.edu)

0094-8276/12/2012GL052811

[1]Auxiliary materials are available in the HTML. doi:10.1029/2012GL052811.

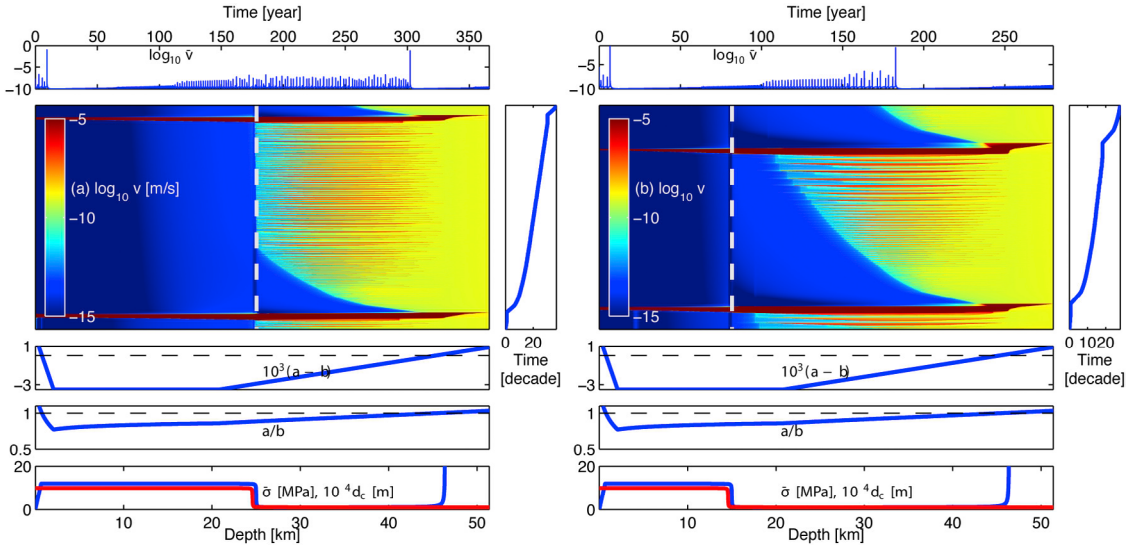

Figure 1. Two modes of SSE triggering dynamic slip events. Top panel shows spatially averaged slip speed with time, showing dynamic events and regularly spaced SSE. Next panel shows space-time distribution of slip rate (logarithmic color scale) with depth scale on bottom. Time (vertical axis, from bottom to top) is proportional to solver time steps; right panel shows the evolution of time with time step. Bottom plots show depth distribution $a - b$, a/b, and $\bar{\sigma}$ (blue) and d_c (red), as a function of depth. (a) Low $\bar{\sigma}$ region extending from 25 to 45 km depth. (b) Low $\bar{\sigma}$ region extending from 15 to 45 km depth.

and v_s are respectively nominal stress, shear modulus, and shear-wave speed. Slip at a constant rate v^∞ is applied below depth $z_{\rm pl} \sim 52$ km. The friction coefficient f is a function of slip speed v (integral of shear strain rate $\dot{\gamma}$ across the shear zone) and state variable θ. We employ the regularized form of the rate-state equations [*Rice et al.*, 2001],

$$f(\theta, v) = a\text{arcsinh}\left[\frac{v}{2v_0} exp\left(\frac{f_0 + bln(\theta v_0/d_c)}{a}\right)\right], \qquad (2)$$

and slip-law state evolution. The heat equation, with thermal diffusivity $c_{\rm th}$, includes shear heating $\tau\dot{\gamma}/\rho c$, where c is specific heat capacity and ρ density. The shear strain-rate is $\dot{\gamma}(x, y, t) = v(x, t)g(y)/h$, where $g(y)$ is a (Gaussian) shaping function, and $\int g(y)dy = h$.

[8] Changes in pore pressure p follow

$$\frac{\partial p}{\partial t} = c_{\rm hyd}\frac{\partial^2 p}{\partial y^2} + \Lambda\frac{\partial T}{\partial t} - \frac{1}{\beta}\frac{\partial \phi}{\partial t}, \qquad (3)$$

where $c_{\rm hyd}$ is hydraulic diffusivity, β is compressibility of the fluid and pore space, ϕ is the inelastic component of porosity, and Λ is the thermal pressurization parameter [*Rice*, 2006]. Dilatancy/compaction acts as a fluid pressure sink/source, and thermal pressurization as a source. We employ a constitutive law for inelastic change in porosity $\delta\phi$, motivated by experiments [*Samuelson et al.*, 2009], that follows *Segall and Rice* [1995], but extended to account for a finite thickness shear zone [*Segall and Bradley*, 2012]. The latter reference also describes the numerical methods employed here.

[9] The distribution of frictional properties loosely follows *Liu and Rice* [2009]. The parameter a ('direct effect') is given by $a = \alpha(T + 273.15)$, where the nominal $\alpha = 3 \times 10^{-5}$, and T is taken from the *Peacock* [2009] geotherm. Lab experiments on gabbros [*He et al.*, 2007] show large scatter, but can be interpreted to show a transition from velocity weakening to strengthening behavior at $T \sim 510°$C. We parameterize $a - b$, which gives the steady-state frictional response, as piecewise linear (Figure 1), with three sections: the shallow (low T) region is velocity strengthening; at intermediate depth $a - b = -3.5 \times 10^{-3}$; while at greater depth friction transitions to $a - b > 0$ at a depth of ~45 km.

[10] Based on seismic imaging studies that suggest near lithostatic pore pressures [*Audet et al.*, 2009], and uniform property simulations [*Segall and Bradley*, 2012], we take $\bar{\sigma} \equiv \sigma - p^\infty$ in the depth range 25 to 40 km to be of order 1 MPa. At seismogenic depths $\bar{\sigma} \sim 12$ MPa, while for $z > 47$ km $\bar{\sigma}$ is ~110 MPa. The Low Effective-Stress Velocity-Weakening (LESVW) region is where SSE are anticipated to nucleate [*Segall et al.*, 2010; *Segall and Bradley*, 2012], and indeed this is observed. Within the LESVW we take $d_c = 100$ μm, increasing for numerical expediency to 1 mm updip (the grid in x would need to be very fine at higher $\bar{\sigma}$). The transition in d_c takes place at least 2 km updip of the transition in $\bar{\sigma}$ to prevent artifacts at the $\bar{\sigma}$ transition.

[11] We found that thermal pressurization overwhelms velocity strengthening friction at depth, causing dynamic ruptures to propagate well into the strengthening region. We thus suppress thermal pressurization at depth where $a > b$. An increase in shear zone thickness would reduce frictional heating; however, we simplify this by artificially increasing the heat capacity. For sufficiently high $\bar{\sigma}$ this is effective at stopping dynamic rupture.

3. Results

[12] Numerical results fall into two classes, depending on the size of the LESVW (labeled W) relative to the drained critical nucleation dimension $L_c = d_c\mu'/(\sigma - p^\infty)(b - a)$, where $\mu' = \mu/(1 - \nu)$. Accounting for incomplete drainage

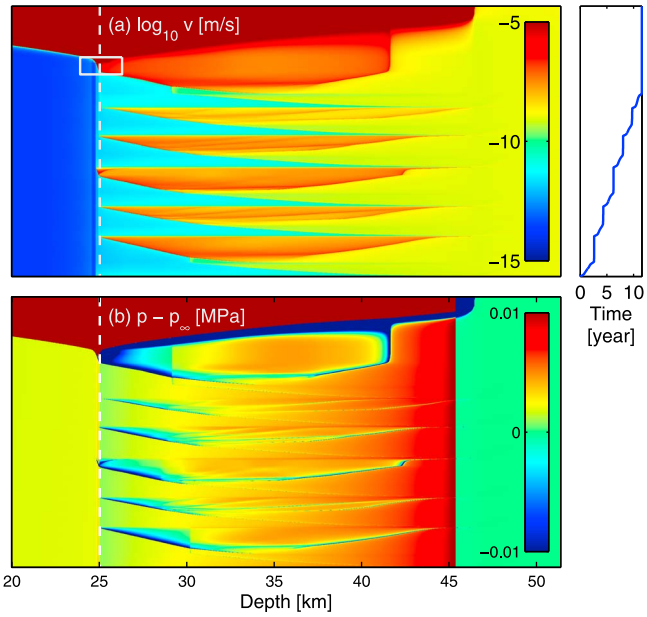

Figure 2. Zoom on Figure 1a. (a) Slip speed and (b) induced pore-pressure change for the last several SSE prior to a dynamic event. Box in Figure 2a shows region in Figure 3. White dashed line shows depth of $\bar{\sigma}$ transition. Horizontal axis is depth and vertical axis is solver time; mapping to physical time in right panel.

does not change this value significantly (see auxiliary material). An example where the LESVW is relatively small (but $W/L_c \sim 30$–50) is shown in Figure 1a. For nearly a century following a dynamic event the fault is relatively quiescent, with creep penetrating updip into the locked zone, at which point slow-slip events (SSE) spontaneously nucleate. Note that, as in many geodetic inversions, there is a "transition zone" between creep at the relative plate velocity, v^{∞}, and the essentially locked fault. In the simulations this transition arises naturally, but is not static; the transition propagates updip as a function of time.

[13] As has been seen in previous simulations of this type [*Segall et al.*, 2010; *Liu and Rubin*, 2010; *Segall and Bradley*, 2012], the SSE are stabilized by dilatancy-induced decreases in pore pressure at the leading edge of the SSE (Figure 2b). This is followed by a very modest increase in pore pressure due to shear heating during the SSE. With time the SSE propagate updip until they hit the boundary where the background effective normal stress increases. In this example, the SSE remain trapped at the boundary of the low $\bar{\sigma}$ region for more than 200 years before a dynamic event occurs (Figure 1a).

[14] The behavior with larger LESVW ($W/L_c \sim 70$) is shown in Figure 1b. Again there is a quiescent period following a dynamic event in which the transition between creeping and locked fault extends updip with time, followed by the spontaneous onset of SSE. The SSE generally propagate farther updip with time, but in this case a dynamic event nucleates before the SSE reach the updip limit of the low $\bar{\sigma}$ region.

[15] Our focus is on how SSE influence the occurrence of dynamic ruptures, which is quite different in the two examples shown in Figure 1. The behavior for the smaller LESVW

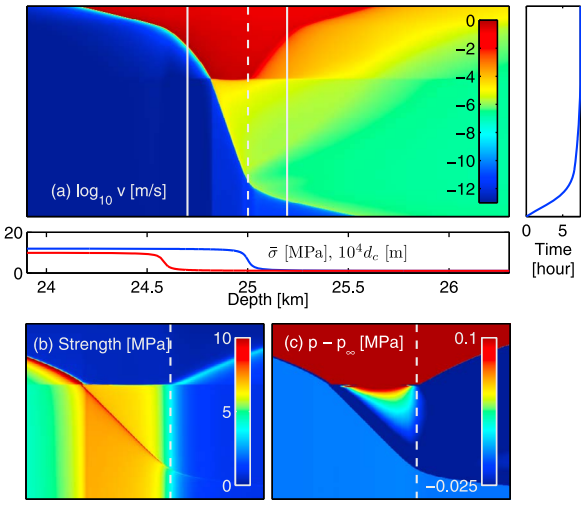

Figure 3. Further zoom in on model in Figure 1a, showing the transition from slow-slip to dynamic rupture. (a) Slip speed, (b) fault strength $f\bar{\sigma}$, and (c) induced pore-pressure change. Horizontal axis is depth; vertical axis is solver time. White dashed line shows depth of $\bar{\sigma}$ transition. White box outlines the region in the top image shown in the bottom images.

region is illustrated in more detail in Figure 3. As successive SSE terminate at the updip end of the low $\bar{\sigma}$ region, they generate a stress concentration within the nominally locked zone. Toward the end of the interseismic cycle, SSE propagate slightly into the higher $\bar{\sigma}$ region. While the details depend on the $\bar{\sigma}$ distribution, slow slip in the high $\bar{\sigma}$ region generates significantly more frictional heat. As the ultimate SSE penetrates the higher $\bar{\sigma}$ region, thermal pressurization

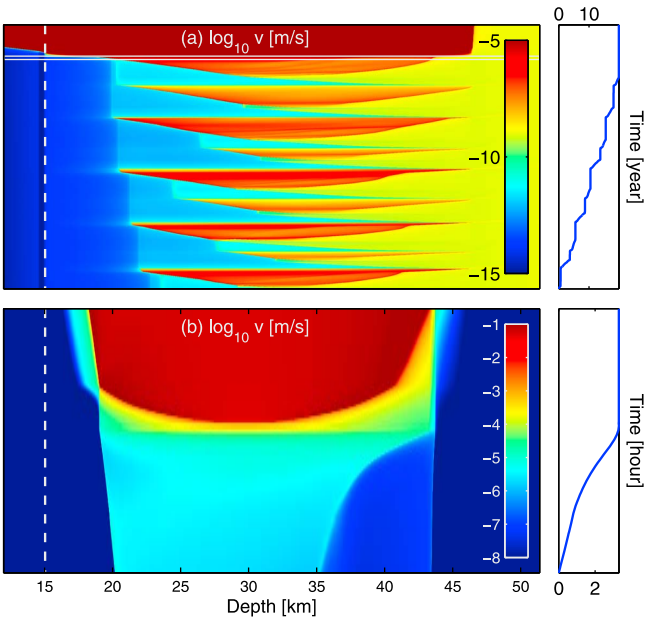

Figure 4. Zoom on Figure 1b, showing slip speed for (a) last several SSE prior to a dynamic event, and (b) period leading up to dynamic event. White dashed line shows depth of $\bar{\sigma}$ transition. White box outlines the region in Figure 4a shown in Figure 4b.

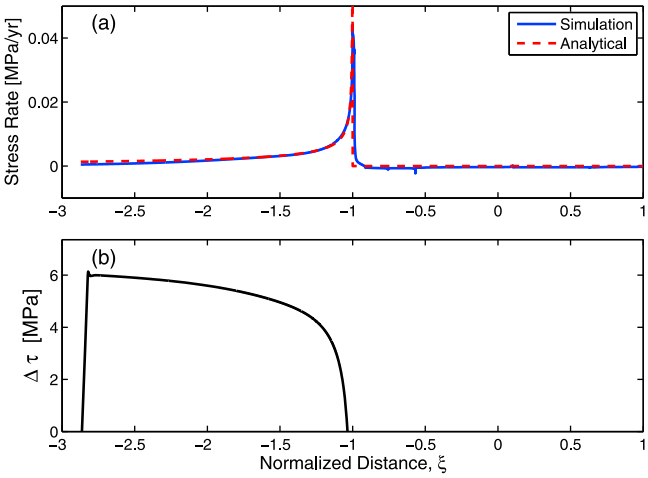

Figure 5. (a) Average stress rate from numerical simulation (Figure 1a) compared with analytical approximation, equation (4). (b) Magnitude of localized stress heterogeneity within locked zone necessary to nucleate an event within 500 years, assuming the width of the heterogeneity exceeds critical nucleation dimension, and residual stress following dynamic rupture is 0.5 MPa, as in simulation results. The decrease in $\Delta\tau$ near the free surface is due to a decrease in frictional resistance $f\bar{\sigma}$; it is also a region where the analytical approximation, which neglects free surface effects, is inaccurate.

induces an increasing loss of strength and the rupture becomes unstable. The ensuing strong stress concentration at the rupture tip allows the dynamic event to propagate into the locked zone with only modest (few MPa) stress drop.

[16] Nucleation of a dynamic event in the larger LESVW case is illustrated in Figure 4. As shown in Figure 1b the SSE generally propagate updip with time. This brings the SSE front into increasingly velocity weakening regions. In addition, the maximum slip speed during SSE is an increasing function of rupture length [*Segall et al.*, 2010], such that the slip speeds increase slightly with time. Although there is no clear increase in maximum slip speed over the last several SSE, increased slip speed enhances thermal pressurization. The onset of the ultimate SSE is unremarkable, and essentially indistinguishable from the preceding events. However, the slip speed eventually reaches a point where thermal pressurization becomes the dominant weakening mechanism [*Schmitt et al.*, 2011]. At this point slip accelerates to inertial speeds *within* the SSE zone, and then propagates updip.

4. Discussion

[17] We have discussed three ways in which SSE can influence the occurrence of earthquakes: 1) static stress perturbations due to SSE cause nucleation of a dynamic event *updip* of the SSE zone; 2) SSE extend partially into the locked, higher $\bar{\sigma}$ region where enhanced weakening causes the rupture to accelerate; and 3) SSE extend gradually updip with time, ultimately initiating dynamic rupture *within* the SSE zone.

[18] Our numerical simulations do not exhibit mechanism 1, presumably because the model is too smooth (both in terms of fault geometry and/or material properties) to induce sufficient local stress concentrations. In the auxiliary material, we show that the stressing rate, $\dot{\tau}$, due to repeated SSE can be approximated by

$$\dot{\tau}(\xi) = -\frac{\mu' v^{\infty}}{2\pi l}\frac{\mathrm{sgn}(\xi)}{\sqrt{\xi^2-1}}, \quad |\xi| > 1 \tag{4}$$

where l is the half-width of the SSE zone, $\xi = x'/l$ is normalized distance from the SSE zone center ($x' = 0$). Equation (4) is in good agreement (Figure 5a) with the average rate of stress accumulation from the time the SSE first reach the updip end of the LESVW region (Figure 1a) to the time just prior to dynamic rupture. Equation (4) can be used to estimate the magnitude of an isolated stress heterogeneity within the locked zone required to trigger a dynamic rupture, assuming that the width of the heterogeneity is sufficiently large to permit unstable slip (that is, the width exceeds some multiple of L_c). Nucleation requires the shear stress to reach the static strength $f_0\bar{\sigma}$. Thus, for a stress heterogeneity of magnitude $\Delta\tau$, an estimate of the time to instability is $\Delta T(\xi) \sim [f_0\bar{\sigma}(\xi) - \Delta\tau - \tau_{\mathrm{res}}]/\dot{\tau}(\xi)$, where $\tau_{\mathrm{res}} \sim 0.5$ MPa is the residual stress after dynamic events. Figure 5b shows that stress concentrations $\Delta\tau$ an appreciable distance from the top of the ETS zone would have to be of order 5 MPa (comparable to an earthquake stress drop) in order to nucleate an instability in ≤ 500 years. While stress concentrations of this scale could arise due to previous partial ruptures [*Lapusta and Rice*, 2003], non-planar fault geometry, or other factors, they do not arise in the simulations here.

[19] With mechanism 3, dynamic events nucleate within the SSE zone. Dynamic rupture within the SSE zone appears to be contradictory to observations from the Nankai region Japan, where the 1944–1946 Tonankai and Nankaido earthquakes apparently occurred updip of the ETS zone [*Dragert et al.*, 2004]. It is possible that fault properties strictly prohibit fast slip within the ETS zone, although that is not the case for the class of models here, and indeed mechanism 2 dynamic events also rupture into the ETS zone (Figure 1a). Increasing the shear zone thickness h within the LESVW region to suppress thermal pressurization does not prevent dynamic events from propagating through the ETS region, at least for the parameter ranges considered. We also examined drained models with a v-cutoff, such that friction becomes velocity strengthening above a critical threshold [*Shibazaki and Shimamoto*, 2007], and find that this too fails to prevent dynamic events from propagating through the ETS region. This occurs simply because the increase in friction f at very low $\bar{\sigma}$ yields a small increase in strength, one that cannot compensate for the large stress drop updip of the ETS zone. Understanding what limits fast slip from penetrating the ETS zone is an important outstanding mechanical problem.

[20] Mechanism 2 is likely the most intuitive. If SSE are limited in depth extent by a change in physical properties and/or background effective stress, the repeated SSE produce a stress concentration at the top of the ETS zone. Limited penetration of the SSE into the higher $\bar{\sigma}$ region causes thermal pressurization that is sufficient to allow rupture to accelerate to inertial limits. It is notable that there does not appear to be any obvious change in SSE behavior prior to the onset of a dynamic event, in terms of repeat time, maximum slip speed, or amount of slip in an SSE.

[21] We can use (4) to make a rough estimate of the recurrence time for dynamic events, assuming that the stress concentration at the top of the SSE region must reach the static

strength over a critical nucleation dimension, which we take to be κL_c. Thus, $\Delta T = f_0\bar{\sigma}/\dot{\tau}(\xi^*) = (2\pi f_0\bar{\sigma}l/\mu'v^\infty)\sqrt{\xi^{*2}-1}$ where $\xi^* \equiv -1 - \kappa L_c/l$. For the simulation in Figure 3 the ultimate SSE penetrates $\sim$ 700 m into the high $\bar{\sigma}$ region ($\kappa \sim 7$). This corresponds to $\xi^* = -1.01$ and a predicted recurrence time of 290 years. This is of the order of the simulated recurrence interval of 300 years, although the simple estimate does not account for the more than 100 years before the SSE actually reach the updip boundary of the LESVW region.

[22] The critical dimension W for the transition in behavior between that observed in Figures 1a and 1b is controlled more by thermal pressurization than dilatancy. Properties are nonuniform so the dimensionless parameters are only approximately defined, but a reasonable estimate is $E_p = 1.4 \times 10^{-3}$, $a/b = 0.95$ (see the auxiliary material for definitions). *Segall et al.* [2010] presented isothermal simulations that show for $E_p = 0.001$ and $a/b = 0.9$, dilatancy stabilizes slip to at least $W/L_c > 20$, and quite likely much more. Thus, it is not surprising that dilatancy can stabilize slip for $W/L_c \sim 30$–50. For the case in Figure 1b the friction becomes more velocity weakening as slip propagates updip. *Schmitt et al.* [2011] compute a critical velocity for which, in the absence of dilatancy, thermal pressurization overwhelms rate-state friction and becomes the dominant weakening mechanism. The behavior is different for aging-law and slip-law friction, but the effect of dilatancy is to make nucleation more like aging law simulations. In this case *Schmitt et al.* [2011] find the critical velocity can be approximated by

$$v_{\mathrm{crit}} \approx \frac{q(a,b)}{\pi d_c}\left[\frac{4\rho c_v\left(\sqrt{c_{\mathrm{th}}}+\sqrt{c_{\mathrm{hyd}}}\right)}{\Lambda f_0'}\right]^2, \qquad (5)$$

where $q(a, b)$ is a function of the rate-state parameters. Note that v_{crit} is independent of normal stress. For $b - a \sim 2 \times 10^{-3}$, *Schmitt et al.* [2011, Figure 13] find v_{crit} on the order of 10^{-5} m/s, which is comparable to the slip speed in Figure 4 at the point slip becomes unstable. Thus, the current simulations are consistent with previous experience and suggest that thermal pressurization induces the dynamic event, rather than W/L_c becoming too large for dilatancy to stabilize slip. We have confirmed this with a comparable simulation of the larger W/L_c case without thermal pressurization; as expected, SSE extend to the updip $\bar{\sigma}$ transition, where eventually the dynamic event nucleates.

5. Summary

[23] Relatively smooth models with depth dependent friction and effective normal stress show that slow-slip events evolve into dynamic ruptures, rather than triggering them by static stress transfer. Two mechanisms are identified, one in which dynamic rupture initiates at the updip margin of the SSE zone, the other in which fast slip initiates within the SSE zone. If either process occurs in nature the probability of a dynamic rupture does increase during ETS events. In neither case, however, is there obvious indication that dynamic instability is imminent prior to the event.

[24] **Acknowledgments.** We thank the two anonymous reviewers for their comments.

[25] The Editor thanks two anonymous reviewers for assisting in the evaluation of this paper.

References

Audet, P., M. G. Bostock, N. I. Christensen, and S. M. Peacock (2009), Seismic evidence for overpressured subducted oceanic crust and megathrust fault sealing, *Nature*, *457*, 76–78, doi:10.1038/nature07650.

Beeler, N. (2012), Re-estimated effects of deep episodic slip on the occurrence and probability of great earthquakes in Cascadia: Delayed failure, *Bull. Seismol. Soc. Am.*, in press.

Brudzinski, M. R., and R. M. Allen (2007), Segmentation in episodic tremor and slip all along Cascadia, *Geology*, *35*, 907–910, doi:10.1130/G23740A.1.

Dieterich, J. (1994), A constitutive law for rate of earthquake production and its application to earthquake clustering, *J. Geophys. Res.*, *99*(B2), 2601–2618.

Dragert, H., K. Wang, and G. Rogers (2004), Geodetic and seismic signatures of episodic tremor and slip in the northern Cascadia subduction zone, *Earth Planets Space*, *56*(12), 1143–1150.

Goldfinger, C., et al. (2011), Turbidite event history: Methods and implications for Holocene paleoseismicity of the Cascadia subduction zone, in *Earthquake Hazards of the Pacific Northwest Coastal and Marine Regions*, edited by R. Kayen, *U.S. Geol. Surv. Prof. Pap.*, 1661-F, 170 pp.

He, C., Z. Wang, and W. Yao (2007), Frictional sliding of gabbro gouge under hydrothermal conditions, *Tectonophysics*, *445*, 353–362.

Lapusta, N., and J. R. Rice (2003), Nucleation and early seismic propagation of small and large events in a crustal earthquake model, *J. Geophys. Res.*, *108*(B4), 2205, doi:10.1029/2001JB000793

Liu, Y., and J. R. Rice (2009), Slow slip predictions based on granite and gabbro friction data compared to GPS measurements in northern Cascadia, *J. Geophys. Res.*, *114*, B09407, doi:10.1029/2008JB006142.

Liu, Y., and A. M. Rubin (2010), Role of fault gouge dilatancy on aseismic deformation transients, *J. Geophys. Res.*, *115*, B10414, doi:10.1029/2010JB007522.

Mazzotti, S., and J. Adams (2004), Variability of near-term probability for the next great earthquake on the Cascadia subduction zone, *Bull. Seismol. Soc. Am.*, *94*(5), 1954–1959.

Ozawa, S., H. Suito, and M. Tobita (2007), Occurrence of quasi-periodic slow-slip off the east coast of the Boso peninsula, central Japan, *Earth Planets Space*, *59*(12), 1241–1245.

Peacock, S. M. (2009), Thermal and metamorphic environment of subduction zone episodic tremor and slip, *J. Geophys. Res.*, *114*, B00A07, doi:10.1029/2008JB005978.

Rice, J. (1993), Spatio-temporal complexity of slip on a fault, *J. Geophys. Res.*, *98*, 9885–9907.

Rice, J. R. (2006), Heating and weakening of faults during earthquake slip, *J. Geophys. Res.*, *111*, B05311, doi:10.1029/2005JB004006.

Rice, J. R., N. Lapusta, and K. Ranjith (2001), Rate and state dependent friction and the stability of sliding between elastically deformable solids, *J. Mech. Phys. Sol.*, *49*, 1865–1898.

Samuelson, J., D. Elsworth, and C. Marone (2009), Shear-induced dilatancy of fluid-saturated faults: Experiment and theory, *J. Geophys. Res.*, *114*, B12404, doi:10.1029/2008JB006273.

Schmitt, S. V., P. Segall, and T. Matsuzawa (2011), Shear heating-induced thermal pressurization during earthquake nucleation, *J. Geophys. Res.*, *116*, B06308, doi:10.1029/2010JB008035.

Segall, P., and A. M. Bradley (2012), Slow vs fast slip due to competition between thermal pressurization and dilatant strengthening, *J. Appl. Mech.*, *79*, 031013, doi:10.1115/1.4005896.

Segall, P., and J. R. Rice (1995), Dilatancy, compaction, and slip instability of a fluid-infiltrated fault, *J. Geophys. Res.*, *100*(B11), 22,155–22,171.

Segall, P., E. K. Desmarais, D. Shelly, A. Miklius, and P. Cervelli (2006), Earthquakes triggered by silent slip events on Kilauea volcano, Hawaii, *Nature*, *442*, 71–74, doi:10.1038/nature04938.

Segall, P., A. M. Rubin, A. M. Bradley, and J. R. Rice (2010), Dilatant strengthening as a mechanism for slow slip events, *J. Geophys. Res.*, *115*, B12305, doi:10.1029/2010JB007449.

Shibazaki, B., and T. Shimamoto (2007), Modeling of short-interval silent slip events in deeper subduction interfaces considering the frictional properties at the unstable-stable transition regime, *Geophys. J. Int.*, *171*, 191–205.